HEADTRACK: TRACKING HEAD ORIENTATION USING WIRELESS SIGNALS

BY

AMOD KANT AGRAWAL

THESIS

Submitted in partial fulfillment of the requirements
for the degree of Master of Science in Computer Science
in the Graduate College of the
University of Illinois at Urbana-Champaign, 2019

Urbana, Illinois

Adviser:

Professor Romit Roy Choudhury

ABSTRACT

Estimating and tracking the head orientation of the user is an important problem for numerous mobile computing applications. Current solutions to the problem require deploying infrastructure (namely, cameras and lasers) along with expensive (IMU) sensors. These infrastructure-based approaches bound the user to a limited area of tracking and also disable portability and mobility of the user.

This work presents *HeadTrack* and explores the feasibility of designing a necklace-like wearable consisting of a headset and a chest-piece that can be used to estimate the user's head orientation using wireless (radio frequency) signals. The core problem presented in this thesis is to accurately estimate multiple distances between the chest-piece on the torso and the headset using the ultra-wide band (UWB) radios. Such a wearable not only enables portability but also mobility by decoupling user's *head motion* from the *body motion*.

Although the ultra-wide band radios have a 1GHz bandwidth and high-speed clocks, they are unable to do *sub-centimeter* ranging. We improve the typical $\sim$10cm accuracy of the UWB radios by introducing a wired path between the transmitters and the receivers to serve as a reference point. We split the signal at the transmitter and route it through the wired as well as the wireless paths to improve the accuracy to about 5mm.

We use ViCon to collect the ground truth for our experiments and evaluate our system. HeadTrack uses an IMU to resolve the phase wrap ambiguities and is able to track the head orientation of the user with an accuracy of 6.5°. HeadTrack provides a wearable, occlusion-free, portable, and cost-effective solution to the problem of head orientation tracking with a bounded and non-diverging error.

To my family and friends, for their love and support.

ACKNOWLEDGMENTS

This work has been done under the guidance of Professor Romit Roy Choudhury. I would like to thank him for all the valuable feedback, academic advice, and discussions throughout the course of my degree. I would also like to thank Ashutosh Dekhne for working with me on this project. *HeadTrack* would not have been possible without him and his expertise in ultra-wide band (UWB) radios and wireless sensing. I truly appreciate his help, effort, and guidance on this work.

I also owe my gratitude to my fellow SyNRG (Systems and Networking Research Group) members including Sheng, Nirupam, Suraj, Daguan, and others for encouraging a very open and conducive working environment. I sincerely value their feedback on all my problems, research ideas, and solutions. I have truly learned a lot from everyone. I would also like to thank my academic advisors at the Department of Computer Science for supporting me with assistantships throughout my program.

Finally, I deeply thank my parents, sister, brother-in-law, and friends for their constant support and motivating me to see that my goals come through. My journey at the University of Illinois at Urbana-Champaign has been a fruitful one, and I have thoroughly enjoyed my time here.

TABLE OF CONTENTS

CHAPTER 1: INTRODUCTION

We are living in an age where technology is more pervasive in our lives than ever before. Personal devices like smartphones, smartwatches, and wearables are rapidly becoming ubiquitous and therefore opening doors to a realm of new unsolved problems in the areas of wireless networking, mobile computing, and mobile sensing. With the onset of the Internet-of-Things, a big part of these problems revolves around managing and analyzing the overwhelming amounts of data produced by the sensors. However, the ubiquity of these technologies also comes with some new opportunities that have remained unexplored so far. The field of data science is maturing rapidly to analyze and understand the large amount of sensor data, however, such ubiquity of sensors, mobile devices and networks has also opened unexplored problems in the domain of environmental sensing itself.

One such sub-area of emerging domains and applications in Internet-of-Things, mobile computing, and next-gen wireless networking is radio-frequency (RF) based sensing. This sub-area is largely focused on using RF signals as a sensor and developing applications where the wireless signals in the environment can be used to not only infer the characteristics of the environment but also precisely track the changes in it.

This work focuses on developing a wearable that uses RF signals to track the orientation of the human head using ultra-wide band (UWB) radios. With the emergence of smart wearables and earables (smart earphones) – we envision a future where our mobile devices will collect information about our hand movements and gestures, our walking patterns, our body movements as well as the orientation and the direction in which we are looking. Head orientation tracking can enable a lot of new smart applications because it provides contextual information on where the user is looking while performing a certain activity. I will delve into some of these applications in one of the following sections.

In the past decade, a lot of interesting problems and solutions in RF-based sensing have come up; some of these problems involve finding the distance between devices using RF signals, or even localizing the position of the user inside the building. Some of the harder problems even involve using reflections of RF signals to track the user's walking trajectory or infer their heartbeat and breathing patterns. This area is rapidly developing and I am convinced that next generation IoT systems will greatly leverage this technology.

1.1 ORGANIZATION

The subsequent chapters of this thesis delve into the ideas of RF-based sensing and their techniques.

Starting with chapter 2, it provides the reader with a relevant background on this niche area of mobile computing and sensing. More specifically, it discusses the oncoming of RF-based sensing, its use for user tracking and localization, a popular radio technology for tracking called the ultra-wide band (UWB), and some of the applications of head orientation tracking. Chapter 3 elaborates on our motivation to develop new solutions for head orientation tracking using RF signals and also discusses how the current solutions fall short.

Chapter 4 explains our system, its design, and the components of the processing pipeline in detail. It provides an overview of the HeadTrack's four-stage processing pipeline followed by technical details for each stage. Chapter 5 elaborates on the implementation of our system and the prototype. It also presents our experiments for the ground truth data collection, a crucial step for evaluation of our system.

Chapter 6 discusses the evaluation of our system and presents several results. The results are followed by the core contributions of this work in Chapter 7. It also answers some of the natural questions that the reader might have, envisions our future work, and concludes the thesis.

CHAPTER 2: BACKGROUND

2.1 RADIO-FREQUENCY SENSING

In 1912, the first patent for echo-location was filed where the sound waves were sent into the water to detect the presence of objects. This technology matured into a fairly popular sensing mechanism which at the time was called SONAR (SOund Navigation And Ranging). Over the next few decades, this technology was applied to air and during the World War II, it came to be known as RADAR (RAdio Direction And Ranging). The core idea behind these developments remained the same: inferring presence of objects and their location based on reflections of a transmitted signal.

Radio-frequency (RF) signals have now been long used for wireless communication. We can observe RF signals all around us in different applications – ranging from long distance communication applications like satellite transmissions (including GPS), cellular networks, WiFi in our homes to personal communication applications like bluetooth on our mobile devices and wearables, and NFC for services like Apple Pay and Google Pay. In most applications today, RF is most commonly used for communication from one device to another.

However, with massive development in wireless technologies, their scale, and its ubiquitous nature, a set of new applications based on propagation properties of the wireless signals have emerged. These new applications use the signals around us to "sense" the objects or even determine the activity that is being performed.

These "objects" for sensing have been changing over time: from icebergs, submarines, and airplanes to objects in today's urban environment including humans, cars, trees, and substances. The most common application of RF sensing that we see today is the whole-body imaging using mmWave at the TSA (Transportation Security Administration) airport checkpoints [1]. The scanner uses a millimeter wave that passes through the person's clothing but reflects off the body and the potential metallic objects. These reflections are then used to create an image of the person with areas of potential threats.

We envision that this is just a start and we'll observe the use of RF sensing in many scenarios of personal use with onset of personalized IoT systems and applications. I will talk about some of the advanced applications that are still developing but already have interesting solutions:

Wireless ranging: Ranging literature in wireless systems primarily focuses on finding the signal's propagation delay using time-of-flight measurements between the radios. There are three major challenges in estimating the propagation delay: 1. since wireless signals travel at the speed of light, ranging requires extremely fast clocks that can measure time of arrival of the signal at nanosecond granularity, 2. since the clocks of two radios are unsynchronized, we need mechanisms to account for clock offsets, and, 3. different clocks have different rates, therefore, even when synchronized - they may drift over time. To completely side-step the clock synchronization process, *two-way ranging* [2] is used where the transmitter (Tx) and the receiver (Rx) symmetrically exchange packets to find the time-of-flight of the signal as well as the delay time within the radios.

Indoor Localization: RF sensing has also been applied to the problem of indoor localization. The goal of this problem is to localize the user in an indoor environment where GPS systems fall short due to attenuation and strong multipath. The signal RSSI along with the angle-of-arrival (AoA) from multiple transmitters (like WiFi APs) can be used to localize a receivers with respect to the their positions [3]. There's also been research that utilizes the reflections of these signals from the human bodies to estimate their location in the room [4].

Substance Identification: RF sensing has also been used to identify the substances through which the signals propagate. LiquID [5] uses ultra-wide band radios to shine signals through a liquid and based on the signal's propagation delay in the liquid, it is able to estimate its complex permittivity. Optical Spectroscopy also entails shining light of different frequencies through a liquid to analyze the absorption and emission behavior of the liquid [6]. Research has also used RFID tags on top of liquid containers to analyze how the signal reflections from the liquid affect the reflection from the RFID tags to identify the liquid.

Passive health monitoring: RF sensing is also being used to extract the information about heart rate along with breathing rate patterns from the reflections of the WiFi signals from the user's body. There's also been research to categorize these reflections to understand the mood and behavior of the person [7].

Activity tracking: Similar to health monitoring, RF signals have also been used to infer the activity that the users are performing. There has been work on recognizing hand or body gestures using RF imaging. The reflections of the signals may be fed into a machine learning model to image the gestures being performed by the user. There has also been work that again uses WiFi reflections to enable fall detection for the elderly inside the homes [8, 9].

2.2 ULTRA-WIDE BAND RADIO

Ultra-wide band (UWB) radios use bandwidth in excess of 500MHz and employ extremely fast clocks to be able to sample and decode signals with such large bandwidths. Large bandwidths and fast clocks make UWB an ideal radio technology for time-of-flight based ranging because it provides a fine-grained view of the channel. The activity on a channel between a transmitter (Tx) and a receiver (Rx) is visualized using the *channel impulse response* (CIR). UWB is a good choice for indoor applications as well because it allows us to separate the first arriving path of the signal from rest of the multipath. In general, like any other radio technology, the distance up to which UWB can successfully receive and decode packets is a function of the transmitter's power. In US, FCC limits the UWB transmitter power to -43.3dBm/MHz in the most regions where UWB frequencies are allowed.

UWB has now been used to track the motion of fire fighters inside the building during an emergency [10], localize the high speed motion of the ball in various sports like baseball [11], localize a person in a room using multiple UWB anchors, or even perform relative localization of multiple people on a common field (particularly useful for battlefields and sports).

2.3 APPLICATIONS FOR HEAD ORIENTATION TRACKING

Contextual information: The head orientation can provide contextual information about the activity that the user is performing. The systems are not only getting smarter but are also being trained to interact with the users. Information about where the user is looking while performing an activity can help these systems infer the user's intent. Earables i.e. smart earphones are now running smart voice assistants like Alexa, Siri, and Google Now on them. The head orientation of the user can be used by the voice assistants to improve their understanding of the user's action and the intended behavior.

A lot of work has been done on indoor localization i.e. finding the location of the user in an indoor environment, where the user's location can help the assistants provide context on her intent. For example, instead of telling Alexa to turn off the *lamp 1*, the user can now be near lamp 1, and Alexa would use the proximity as a feature to turn off that specific lamp. However, what if the user is near multiple lamps? HeadTrack can provide additional context and help Alexa know which lamp is the user looking at. Hence, Alexa can use proximity as well as the head orientation as features to enable location and orientation-based intelligent

commands. Similarly, if the user tells the Alexa to add 30 seconds to the timer. Alexa can disambiguate whether the user's intent is meant for the microwave or for the oven, based on the location and the head orientation.

Driving safety: An important application of head orientation tracking lies in driving safety systems. Driving safety systems monitor the driver's head motion to make sure that the driver is not only attentive but also is checking the mirrors frequently. In case the driver is feeling sleepy or not consistently looking at the road, the system can warn the driver. It can also be used by fleet owners to make sure that their drivers are attentive and therefore incentivize safe driving.

Aviation: Application of head orientation also lies in the aviation industry, especially air force jets which fly at a very high speed. IMUs in such scenarios cannot work at all because they can't measure gravity and is polluted by the linear acceleration of the jet. The aviation industry aims to build smart cockpits that can react to the direction in which the pilot is looking. Head orientation tracking is an important problem in this domain and requires a solution that doesn't depend on IMU.

Augmented and Virtual Reality (AR/VR) systems: One of the biggest applications of head orientation tracking lies in AR/VR systems. These systems require very accurate and precise head orientation of the user to be able to create a seamless and immersive experience.

Sport Analytics: Another application of head orientation involves helping athletes analyzing their reaction speeds while playing. Professional players can use HeadTrack to see how fast can they react to the game. IoT is already being used to track the equipments such as bats, balls, and rackets. Providing more context about the player's field of vision can also help improve these analytics.

CHAPTER 3: MOTIVATION

With the onset of advanced applications that require head orientation tracking, we revisit existing solutions to the problem. On deeper analysis, we find that current tracking solutions either require expensive sensors or need to deploy infrastructure to solve the problem.

3.1 CURRENT TRACKING SOLUTIONS

3.1.1 Inertial tracking using IMU

Inertial tracking uses data from the Inertial Measurement Unit (IMU) sensors which consists of accelerometer, gyroscope, and magnetometer. Accelerometers measure the acceleration of the device whereas the gyroscope measures the angular velocity (rotation) of the device and the magnetometer uses the Earth's magnetic field to measure the intensity of the magnetic vector pointing towards the magnetic north. Fusing different data streams from these sensors (also called sensor fusion) is used to track the orientation, position, and location of the device. This technique is often referred to as **dead reckoning** in the community.

The IMU sensors measure the acceleration, angular velocity and the magnetic vector with respect to their own local frame of reference (LRF). Constant global "anchors" like gravity and magnetic north vector are used to project the IMU data from its local frame of reference to the global frame of reference. With the acceleration in the global reference frame, we can integrate it to find velocity and double integrate it to find displacement of the object. Summarizing, to track the object in a 3D space - the inertial tracking algorithm must keep a track of the orientation of the device at all times to be able to project its acceleration to the GRF and double integrate to find the displacement. There has been a lot of work in this area that has focused on improving localization error [12, 13, 14].

3.1.2 Vision-based tracking

Vision-based tracking is one of the most widely used solution in systems for virtual and augmented reality (VR and AR). Most vision-based techniques use vision algorithms and require infrastructure specifically tracking devices such as visible or infrared cameras, a stereo camera system, or a depth camera.

Outside-in tracking: Most of these techniques use markers on the tracking objects, these markers (active like LEDs or passive) are tracked using cameras. Algorithms like POSIT [15] can use data from these cameras to find the position of the object in space. Such tracking techniques are generally called Outside-in tracking. VR systems like PlayStation VR, HTC Vive [16], Oculus Rift [17] use such techniques to localize the user and their head orientation.

Inside-out tracking: These techniques involve having cameras (visible, depth, and Infrared) mounted on the device and the stationary trackers placed in the environment. The position in space is calculated by the device by tracking these markers in the environment. AR and VR systems like Microsoft HoloLens and Oculus Rift S use such techniques to localize the user and their head orientation.

3.1.3 Wireless and Acoustic Tracking

Little work has been done to use RF signals or acoustic signals to track head orientation. These techniques have been widely used in user localization and tracking, however, due to large errors have not been applied to the problem of head orientation tracking.

3.2 CHALLENGES

3.2.1 Inertial tracking

Inertial tracking algorithms require estimate of orientation as well as the location of the object. To estimate orientation, inertial tracking uses gravity and magnetic north vector as "anchors". Therefore, to find the misalignment of the device's local reference frame $\langle x, y, z \rangle$ with the global reference frame $\langle East, North, Up \rangle$, the IMU can measure the direction of the gravity and the magnetic north vector. However, when the device is in motion the gravity measurement is polluted by the linear acceleration of the device. Therefore, it's only possible to find the orientation of the device at instances when the device is static. In between these static instance, the gyroscope is used to measure the rotation about the local axes by integrating the angular velocity. While in theory, the inertial tracking algorithm will suffice the IMU sensors have noise and errors. While integrating the gyroscope, these errors can accumulate over time and hence, must be reset back to zero by using the gravity and magnetic north as anchors. Similarly, double integrating accelerometer will exponentially accumulate errors, however, due to lack of anchors to reset the location error - the location estimate error will continue to diverge unboundedly [18].

3.2.2 Vision-based tracking

While Vision-based tracking methods work very well and are even able to localize markers with an accuracy of less than a millimeter, they not only depend on expensive hardware (like cameras, depth-sensors, IR LEDs, and markers) but also require deployment of infrastructure. In case of outside-in tracking, cameras need to be deployed in the room to be able to track the user whereas in the case of inside-out tracking, markers need to be deployed in the environment. New algorithms may learn features in the environment and use them as markers, however, are computationally expensive for mobile and IoT devices. Vision-based systems may also fail due to occlusions and poor lighting conditions. The deployment of infrastructure not only make these solutions expensive but also inhibit portability and mobility for the user.

3.2.3 RF-based tracking

The biggest challenges in RF-based tracking stem from the unsynchronized clocks between the ranging devices and the strong environmental multipath. Since the RF signals travel at the speed of light, it is essential to have the ranging devices' clocks synchronized at the picosecond granularity to be able to do sub-centimeter ranging. Since RF signals are usually transmitted omnidirectionally, they can bounce off various surfaces and recollect at the receiver with different magnitudes and phases (because of path differences). These properties can account RF tracking to be a hard problem to solve.

CHAPTER 4: SYSTEM DESIGN

4.1 WEARABLE DESIGN

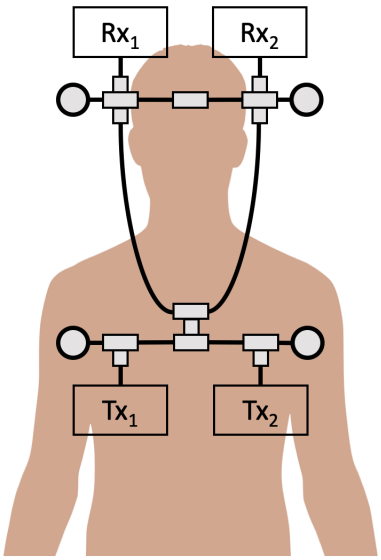

Figure 4.1: HeadTrack's schematic diagram

In this work, we present HeadTrack, a wearable setup that comprises of a headset and a chest-piece which uses ultra-wide band (UWB) radios to track the user's head orientation. We envision this setup as a wearable where the chest-piece can be worn on the body of the user (for example, it can be clipped on the shirt) and depending on the application, the headset radios can be present in different devices like headphones (or other earables), VR/AR headsets, or even spectacles, hats, and helmets. The radios on the chest-piece are connected to the radios on the headset with a wire, this would make our setup a necklace-like wearable that can be conveniently worn in public spaces enabling mobility as well as portability.

The core idea behind this setup is to use ranging between the transmitters located on the chest and the receivers on the headset to find the distances between the points on the torso and points on the headset. We use these pairs of distances between the chest-piece and the headset to infer the head orientation of the user.

4.2 SYSTEM OVERVIEW

Our HeadTrack setup comprises of two major components, a headset and a chest-strap. The headset has two ultra-wide band receivers which are connected to the two ultra-wide band transmitter at the chest-piece using a wire. Figure 4.1 shows a schematic diagram of our setup.

We perform distance ranging between the transmitters on the user's chest and the receivers on the headset. We derive from wireless ranging literature to actively measure distances between the two components based on the time-of-flight (ToF) measurements of the wireless signals transmitted between them. Since electromagnetic waves travel at the speed of light (3×10^8 m/s), measuring time-of-flight accurately requires very high clock sampling rates [19]. Radios that work with large bandwidths, such as ultra-wide band (UWB) radios, naturally have very high sampling rates and therefore are particularly useful for ranging applications. We use a commercial off-the-shelf UWB device that uses a bandwidth of 1 GHz and is able to provide 10cm of ranging accuracy [20]. While a ranging accuracy of 10cm may suffice for most ranging or localization problems, we require accuracy of less than 1cm to develop applications for RF-based head orientation tracking. Fortunately, unique opportunities arise due to the vicinity of system components which allows us to use relative ranging techniques [5] by connecting the transmitters and the receivers with a wire.

The key idea behind improving the accuracy of distance measurements is to enable a second *wired path* between the transmitters and the receivers. As the user head moves in various orientations, the distances between the ranging devices change: which causes change in the signal's wireless propagation delay but not in the wired propagation delay. Hence, the wired signal path provides a reference path and rather than measuring absolute time-of-flight (ToF) between the ranging devices, we can now measure the relative time-of-flight (RToF) of the wireless path with respect to a pre-calibrated wired path with a higher degree of accuracy.

Traditionally, in active wireless ranging systems, a two-way message exchange is typically used which is also called as two-way ranging [2] to find the absolute ToF using unsynchronized clocks. However, due to introduction of the reference path, we are only required to find the relative ToF between the wired and wireless path – hence, a one-way transmission suffices. This also helps us increase our rate of ranging packets and its update rate.

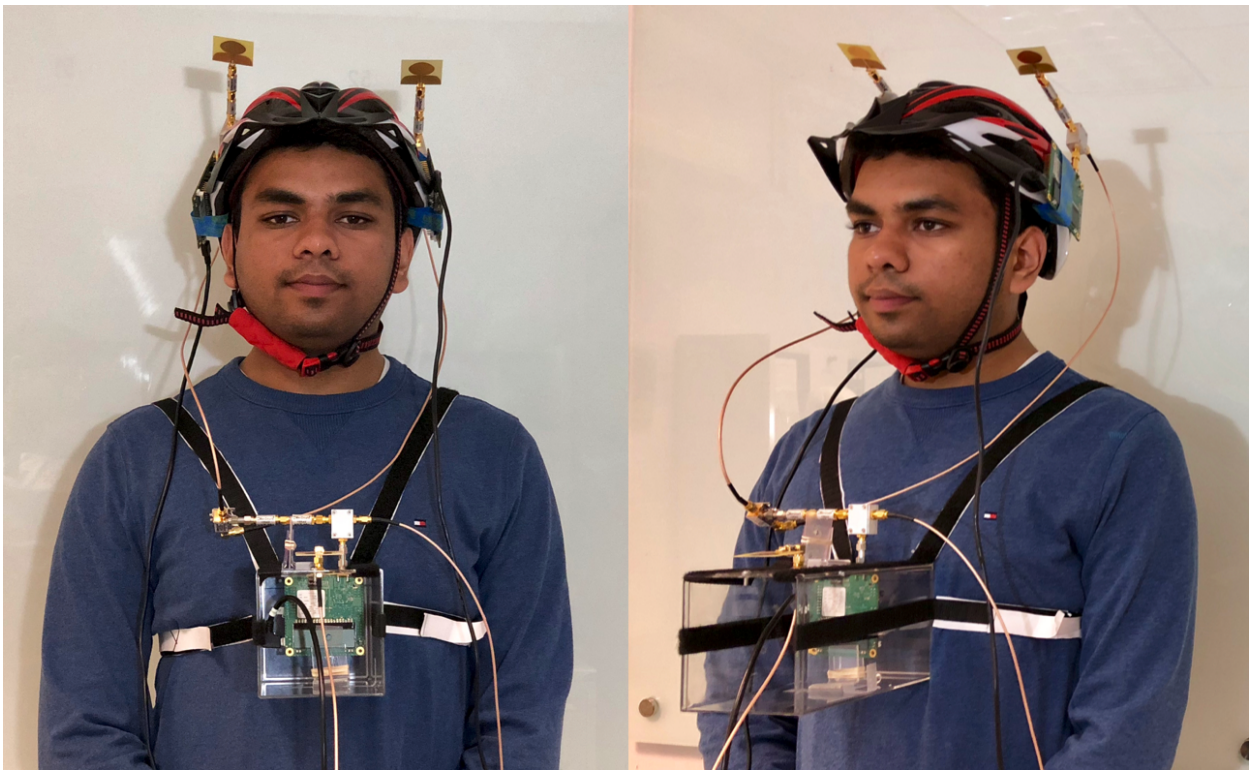

Figure 4.2: Human user wearing the HeadTrack prototype

Figure 4.2 shows our actual prototype strapped on to a human body like a wearable. The computation pipeline underlying HeadTrack is divided into four stages. We present each stage in technical detail in following sections, starting with our results from simulation.

4.3 SIMULATION

We start with simulating the human head motion model in MATLAB. To minimize the cost of the system, we start with one transmitting radio at the chest-piece and two receivers at the headset. Figure 4.3 shows a schematic diagram of our initial setup and defines one pair of distances: $d_{T\text{-}R1}$and $d_{T\text{-}R2}$. This pair of distances is used to run a MATLAB solver to localize the points on a 3D sphere that simulates the model for all possible head orientations. Figure 4.4 shows the results of the solver. We can infer that for a given pair of distances, we can have multiple solutions which lie on a circular locus. Therefore, the same pair of distance measurements between the ranging components can emanate from multiple orientations of the head. This simulation and its results prove that one transmitting radio along with the two receivers are not enough to unambiguously localize the receivers.

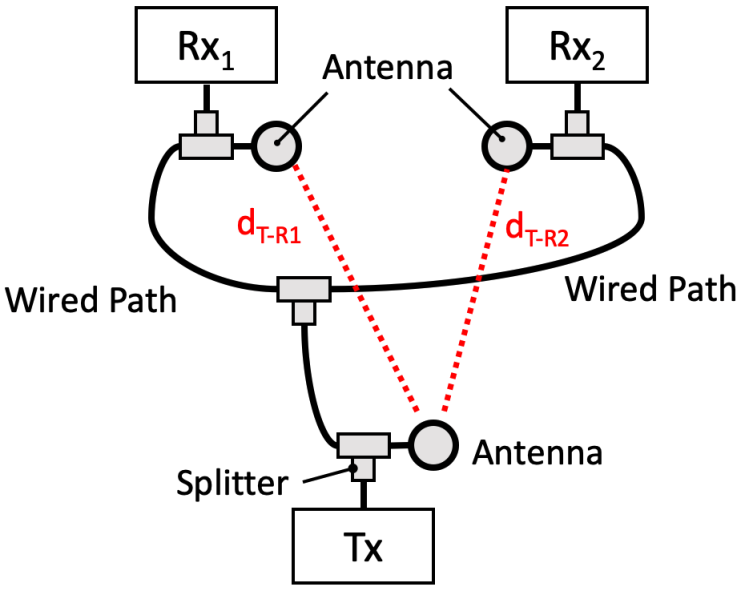

Figure 4.3: HeadTrack's initial setup with one transmitter and two receivers: showing the two distances between the ranging components

To solve this problem, we introduce one more transmitter at the chest-piece which makes our updated system design involve two transmitters at the chest and two receivers at the headset.

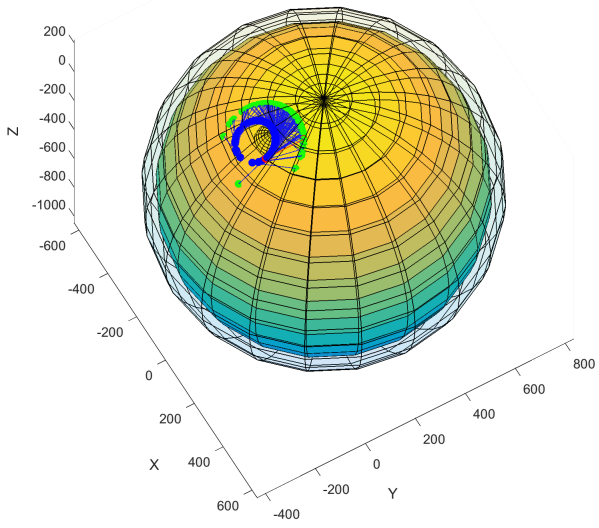

Figure 4.4: Results of the orientation solver shows ambiguity on a circular locus: two pair of distances are not enough to unambiguously solve the localization problem

Given the motion model and limitations of the human neck, our simulation results show that two pairs of distances: ($d_{T1\text{-}R1}$,$d_{T1\text{-}R2}$) and ($d_{T2\text{-}R1}$,$d_{T2\text{-}R2}$) are able to unambiguously solve the localization problem with a unique solution on the sphere.

4.4 SYSTEM STAGES

Recall from Figure 4.1 that we have two transmitters on the chest-piece and two receivers on the headset. The radios are connected by a wire that serves as a latency reference. The transmitter (Tx_1 and Tx_2) forks the signal and sends it over two channels: the wired path as well as the wireless path. The receivers (Rx_1 and Rx_2) receive both the signals over separate channels. For each measurement, we produce a *channel impulse response* (CIR) that plots the signals received at the receiver over time (more precisely, taps) as shown in Figure 4.5. The first peak in the CIR represents the signal that travelled through the wired path and the second peak represents the same signal that travelled through the wireless path.

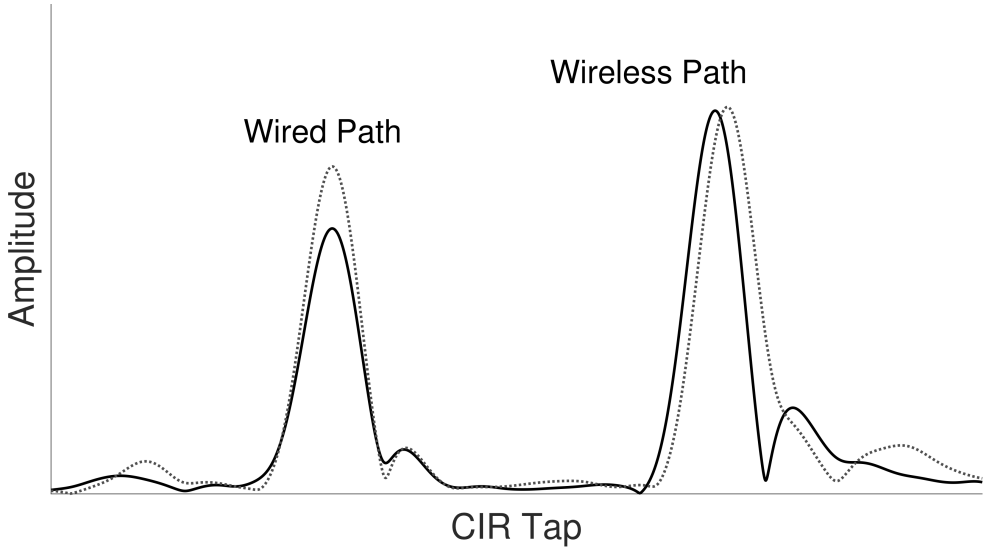

Figure 4.5: Channel Impulse Response (CIR) at the Rx showing two peaks

We use the *Decawave* UWB radios [21] which have a 1GHz bandwidth and a fast clock, therefore, the CIR taps (on X-axis) are at a time gap of 1 nanosecond. The UWB board performs fractional optimizations [22] and brings the ToF precision down to around 350 picoseconds. This implies if we can precisely measure the time of arrival of the signal, our error using ToF measurement would be around 10cm. While this error can suffice for most ranging and localization problems, we require an error of <1cm to precisely track the small changes in head orientation. This motivates the core problem of significantly improving the

time-of-flight measurements [5].

Stage 1: The signal that travels through the wireless channel experience *multipath* which means that the receiver actually receives multiple copies of the same signal. The source signal is transmitted omnidirectionally and bounces off various surfaces to reach the receiver with different delays (corresponding to different paths). Our goal in Stage 1 is to infer the arrival time for the line-of-sight (LoS) signal because it accurately represents the distance between the transmitter and the receiver. Since the nanosecond resolution of the decawave CIR is inadequate, we first perform time-domain interpolation on the CIR. The interpolation process adds multiple samples between the adjacent CIR taps and also interpolates the phase values at each tap.

The next step in this stage is to identify the arrival time of the wireless path in the CIR precisely. To do that, we extract the portion of the CIR that corresponds to the wired path and correlate it with the rest of the CIR. The point at which the correlation peaks is the point (in sub-nanosecond) where the wireless path arrives (T_{signal}). The key observation is that the wireless path's CIR peak is often polluted by the multiple copies of the source signal received at the receiver. The resultant CIR peak is the aggregated peak of the multipath is often not the point of arrival for the LoS signal.

Stage 2: To translate T_{signal} into the absolute time-of-flight of the LoS signal, the clock at receiver (Rx) must be precisely synchronized with the clock at the transmitter (Tx). However, like discussed before, we need 30 picosecond resolution to be able to bring the overall error down to less than 1cm which is not possible with the decawave's clock synchronization system [23]. Hence, the only way to solve this problem is to use relative time-of-flight (RToF) measurements using the reference wire. To completely sidestep the absolute ToF computation, we introduce a calibration step: where we learn the $T_{calibration}$ when the user is stationary and facing at 0° i.e. $\langle yaw, pitch, roll \rangle$ is $\langle 0, 0, 0 \rangle$. Figure 4.6 shows yaw, pitch, and roll for head orientation along with the local frame-of-reference of the user. We now have RToF measurements for both T_{signal} and $T_{calibration}$ with respect to the wire. We use the calibration step to find the distances with respect to the 0° position. Hence, our goal is to find (T_{signal}- $T_{calibration}$) using the RToF measurements (T_{signal}- T_{wire}) and ($T_{calibration}$- T_{wire}).

$$\Delta T = T_{\text{signal}} - T_{\text{calibration}} = (T_{\text{signal}} - T_{\text{wire}}) - (T_{\text{calibration}} - T_{\text{wire}}) \tag{4.1}$$

As shown in equation 4.1, we subtract the RToF measurements to get the relative ToF measurement of any signal with respect to the calibration signal. ΔT gives us the change in

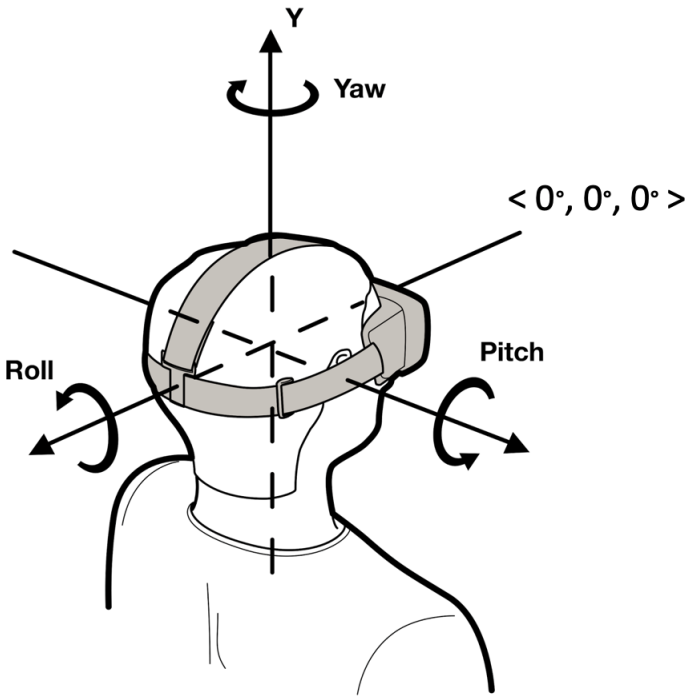

Figure 4.6: Human head motion: Yaw, Pitch, and Roll - showing calibration position

distance with respect to the distance at 0° position.

Stage 3: This stage of our pipeline focuses on using the phase information from the received signal to refine the ToF measurements. The phase information can be extracted directly by the measurement at the receiver or by deriving phase value from the RToF measurements. This also introduces an integer ambiguity problem, that is, it's not possible to know how many wavelengths (n times λ) has the wave traveled to reach the receiver with the measured phase $\hat{\phi}$.

Stage 4: This stage of our pipeline involves removing ambiguities using the data from the IMU (inertial measurement unit). We solve the integer ambiguity problem from the Stage 3 and translate the estimated distances between the transmitters and the receivers to the head orientation in degrees with respect to the origin defined earlier.

We now talk about the implementation of the four stages in detail.

4.5 STAGE 1: INTERPOLATION AND TEMPLATE MATCHING

The *channel impulse response* of a channel between a transmitter (Tx) and receiver (Rx) visualizes the strength and delays of the various copies of source signal received at the Rx. When a signal is transmitted omnidirectionally at the Tx, it travels through different paths and bounces off different surfaces at various angles to reach the receiver. At the Rx, these copies are usually displaced in time but get mixed in the resulting received signal. Figure 4.7 shows the $\text{CIR}_{\text{signal}}$ from the Decawave hardware, where the resolution of the X-axis (a function of bandwidth) is 1nanosecond [21]. Among the various paths that the transmitted signal might take to get recollected at the Rx, one path travels in line-of-sight (LoS) and accurately represents the time-of-flight (and the distance) between the Tx and the Rx. The problem we are trying to solve in this stage is that the LoS signal might arrive at any time between our CIR samples because have a *1ns* granularity. To solve this problem, we create a higher resolution CIR by interpolating it.

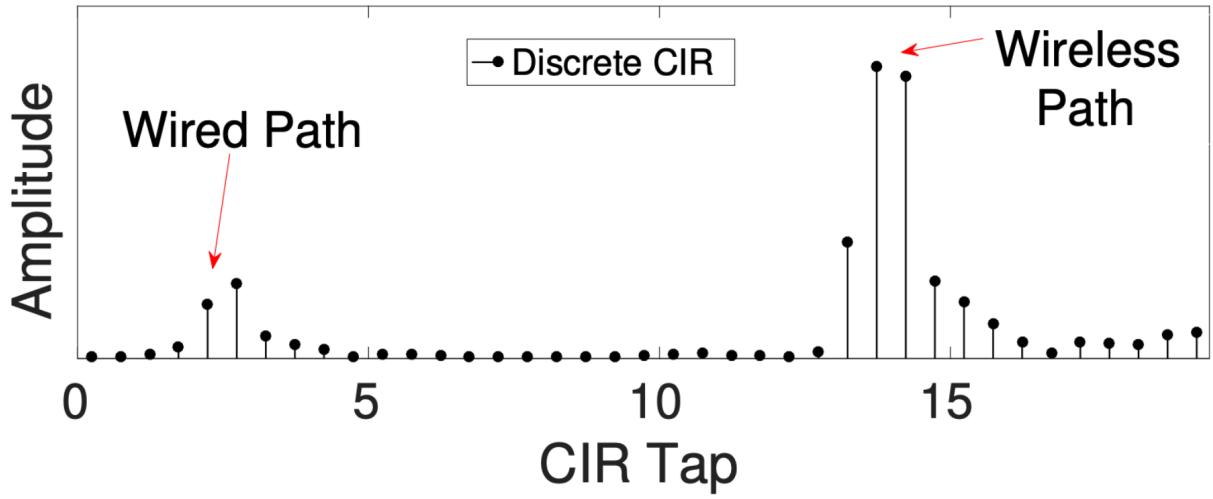

Figure 4.7: Discrete $\text{CIR}_{\text{signal}}$ from decawave with 1 nanosecond tap resolution

Interpolation: We up-sample the CIR by adding zeros between the existing samples followed by applying a 1GHz low pass filter. Figure 4.8 shows an interpolated CIR example which clearly shows that the highest point in the CIR also moves during the interpolation process. It is important to note that this interpolation is also applied to the complex part of the CIR and therefore offers the correct phase at the intermediate interpolated points as well. To put it simply, this interpolation process takes the CIR closer to its original analog version enabling better estimation of LoS time-of-arrival and magnitude.

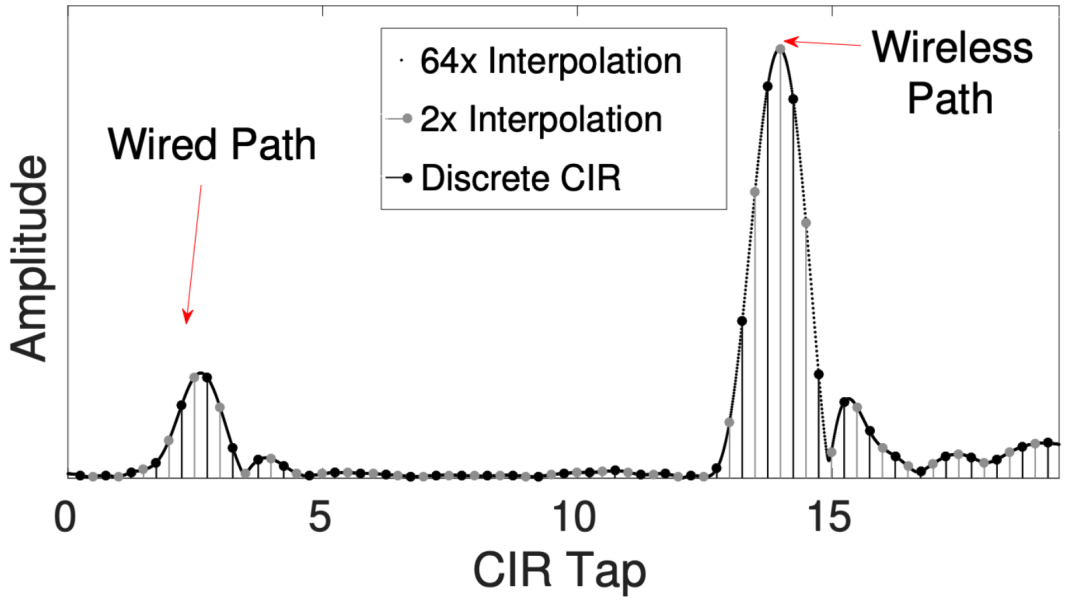

Figure 4.8: Interpolated $\text{CIR}_{\text{signal}}$ to improve tap resolution – black dots represent the original discrete CIR; Big grey dots represent the 2x interpolated CIR i.e. adding one interpolated point between two discrete CIR points; Small grey points represent 64x interpolated CIR i.e. adding 64 interpolated points between two original discrete CIR points

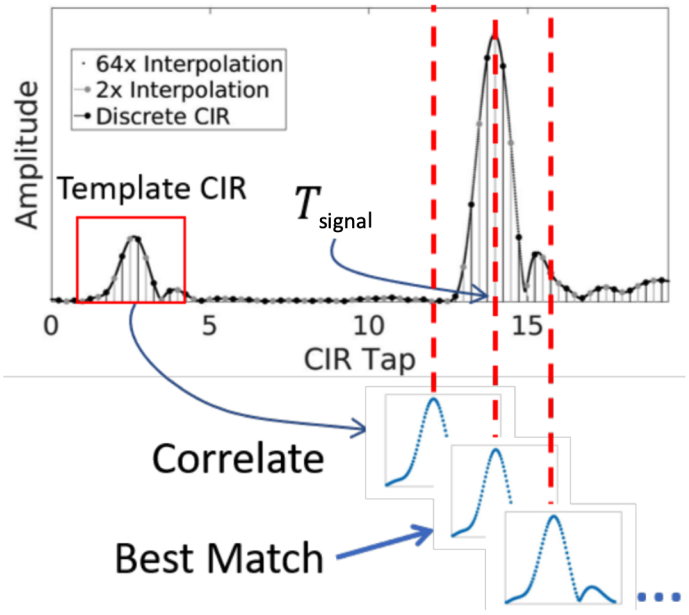

Figure 4.9: Peak detection algorithm (template matching): Template CIR is used to correlate with rest of the CIR to find the precise time-of-arrival (ToA) of the wireless path. The point at which the correlation value peaks is marked as the ToA point.

Template Matching: Now that we have a higher resolution CIR with a sub-nanosecond time axis, it is still polluted by the environmental multipath and the noise from the hardware distortions. Every multipath sample adds a *Sinc(.)* function around the time of arrival of the LoS signal, hence, the tallest peak in our CIR seldom corresponds to the LoS signal. The reference wire between the Tx and the Rx is again used to solve this problem as the signal traveling through it doesn't experience multipath. The CIR from the wired connection is unpolluted of the multipath and captures all the hardware noise at the receiver as well. We call it the *template CIR* because we use this CIR as a template to correlate it with the wireless path's CIR and the sample where the correlation peaks is declared as the point of arrival of the LoS signal. Figure 4.9 shows the template matching process to find the time-of-arrival (ToA) for the LoS signal.

4.6 STAGE 2: DOUBLE DIFFERENCING

Double Differencing ToF: Our ultimate goal is to calculate the distance between the Tx-Rx pairs, which comes from the precise time-of-flight (ToF) measurements of the LoS signals. Equation 4.2 shows how to calculate the distance between the Tx and Rx with the ToF, where $c = 3{\times}10^8$.

$$d_{\text{Tx-Rx}} = (ToF)_{\text{LoS}} \times c_{\text{light}} \tag{4.2}$$

Let T_{signal} be the time-of-arrival of the wireless path at any ranging instance, and T_{wire} is the time-of-arrival of the wired path. T_{wired} would remain fixed (pinned in the CIR at one position) for all ranging instances, T_{signal} would change as the user moves the head in various orientations. If the clocks of the transmitter and receiver were synchronized, we could calculate Tx-Rx time-of-flight using T_{signal} itself. Decawave has a sophisticated clock synchronization system but falls short to achieve synchronization at the picosecond level. This motivates us to develop a technique that be synchronization-free. Fortunately, good opportunity arises to use the T_{wire} as a reference and express other ToFs with respect to it as shown in equation 4.3 and equation 4.4.

Calibration: We introduce a calibration step where we learn the time-of-arrival of the signal ($\text{T}_{\text{calibration}}$) when the user is looking forward with zero yaw, pitch, or roll. We define this point as origin of our system and find the time-of-arrival (T_{signal}) at any ranging instance with respect to the $\text{T}_{\text{calibration}}$.

$$\Delta T_{wire}^{calibration} = T_{calibration} - T_{wire} \tag{4.3}$$

$$\Delta T_{wire}^{signal} = T_{signal} - T_{wire} \tag{4.4}$$

However, ΔT_{wire}^{signal} is not just the time taken for the signal, it also includes the propagation delay through the antenna connectors.

$$\Delta T_{wire}^{signal} = \frac{2L_{ant}}{v_{wire}} + \frac{L_{air}^{signal}}{c} \tag{4.5}$$

$$\Delta T_{wire}^{calibration} = \frac{2L_{ant}}{v_{wire}} + \frac{L_{air}^{calibration}}{c} \tag{4.6}$$

where L_{ant} is the length of the antenna connectors, v_{wire} is the velocity of the signal through the wire, $L_{air}^{calibration}$ is the measured distance between the Tx-Rx during the calibration step, and L_{air}^{signal} is the unknown distance between the Tx-Rx at any ranging instance.

Therefore, we can use the RToF measurements to find the ToF of signal relative to the calibration signal as shown in equation 4.5:

$$\Delta T_{calibration}^{signal} = \Delta T_{wire}^{signal} - \Delta T_{wire}^{calibration} = (T_{signal} - T_{wire}) - (T_{calibration} - T_{wire}) \tag{4.7}$$

$$\Delta T_{calibration}^{signal} = \frac{L_{air}^{signal}}{c} - \frac{L_{air}^{calibration}}{c} \tag{4.8}$$

We use these equations to find the change in the two pairs of distances: *($d_{T1\text{-}R1}$, $d_{T1\text{-}R2}$)* and *($d_{T2\text{-}R1}$, $d_{T2\text{-}R2}$)* from the two transmitters (Tx_1 and Tx_2) at the chest-piece to the two receivers (Rx_1 and Rx_2) at the headset with respect to the calibration point.

$$\Delta d_{Tx-Rx} = \Delta T_{calibration}^{Tx-Rx} \times c \tag{4.9}$$

Double Differencing Phase: The double differencing operation doesn't particularly introduce errors in ToF and the source of ToF errors still lie in the interpolation and templating matching process. The increased multipath can cause the wireless peak to get polluted and hence, immensely affect ToF measurements. Phase brings value to the solution because it is an attribute of the original infinite bandwidth impulse that was obtained even before filtering at the receiver and hence, the phase under the peaks in the CIR is relatively constant. To apply phase, we must differentiate it with respect to the calibration signal as well. The equations 4.10 and 4.11 show double differencing of phase at the receiver, which is very similar to double differencing ToF.

$$\Delta \phi_{wire}^{calibration} = \phi_{calibration} - \phi_{wire} \tag{4.10}$$

$$\Delta \phi_{wire}^{signal} = \phi_{signal} - \phi_{wire} \tag{4.11}$$

$$\Delta\phi^{signal}_{calibration} = \Delta\phi^{signal}_{wire} - \Delta\phi^{calibration}_{wire} \tag{4.12}$$

However, since the phase wraps at 2π, it introduces an integer ambiguity to the number of times the wave has travelled the distance λ. ToF variations can particularly affect the next stage.

4.7 STAGE 3: TIME OF FLIGHT REFINEMENT

While improved ToF precision may be a good start, we now direct our focus to use the carrier phase information observed from the channel impulse response. Recall that CIR is a complex number, therefore, we have a magnitude and a phase value at every tap. The RF transmitter and receiver may have arbitrary phases and therefore, it's difficult to use this information unless we have a reference to differentiate it with.

Stage 3 uses the relative phases obtained from the last step to refine the relative ToF (RToF). Since the phase exhibits a better precision than ToF, there's an opportunity to use the phase information to refine the ToF measurement. Note that the RToF must be a function of distance traveled by the signal which equals an integer multiple of λ plus measured phase $\hat{\phi}$.

$$RToF = \Delta T^{signal}_{wire} = (n + \frac{\hat{\phi}(mod 2\pi)}{2\pi})\frac{\lambda}{c} \tag{4.13}$$

where n is a an integer, $\hat{\phi}$ is the measured phase value at the receiver, λ is the wavelength of the signal, and c is the velocity of the signal in air.

The wired connection between the Tx and the Rx in our case can serve as a reference. In our CIR, we have two peaks corresponding to the wired connection and the wireless connection. While the phase at either of the peaks is arbitrary, the relative phase between the two peaks ($\Delta\phi$) directly correlates to the relative time (ΔToF) between them. Our ultimate goal is to estimate $\hat{n} = n + 1$ or $n - 1$ to get closer to $\Delta\phi^{signal}_{wire}$.

Therefore,

$$RTOF_{refined} = (\hat{n} + \frac{\Delta\phi^{signal}_{wire}}{2\pi})\frac{\lambda}{c} \tag{4.14}$$

However, the phase wraps at 2π and therefore, multiple distances ($n \times \lambda + \phi$) can have the same phase value. This is what we call the *integer ambiguity* of the phase measurements. In the following section, we discuss how we solve the **integer ambiguity problem**.

4.8 STAGE 4: REMOVING AMBIGUITIES

As discussed in the previous section, time-of-flight (ToF) refinement can increase precision but suffers from the problem of integer ambiguity. Increased multipath reflections can increase the variations in ToF measurements causing the system to choose a wrong value for n and snapping the ToF to value that is off by a distance of λ. Since, it is crucial for us to resolve the integer ambiguity correctly, we use an IMU sensor at the headset.

We use the IMU to estimate the orientation of the helmet and not for localization. The IMU sensor consists of an accelerometer, a gyroscope, and a magnetometer. It reads the data from these sensors in its local reference frame (LRF) defined by $\langle x,\ y,\ and\ z \rangle$ axes. The *orientation* of the IMU can be defined as the 3D misalignment of the device's local reference frame with the global reference frame (GRF) defined by $\langle North,\ East,\ and\ Up \rangle$.

To estimate the orientation of the device, gravity and magnetic north readings are used as "anchors". However, if the device is in motion: the gravity value is polluted by the linear acceleration of the device. Therefore, the anchors can only be used to reset the orientation error at time instances when the head motion is static. Between the points of time when the head motion is static, gyroscope is used to track the rotation of the devices in all axes. The gyroscope reads the angular velocity of the device about all the axes in the LRF. To find the rotation (and the orientation), we *integrate* the gyroscope values over time. Since gyroscope values may have noise and errors at each time instant, the integration of these values may accumulate error. To keep the error bounded, it must be reset using the gravity and magnetic north as anchors, whenever the head motion is static.

Using the orientation of the IMU, we find the *euler angles* i.e. the angles that the device makes with all the axes in the global reference frame. The integer ambiguity would result in distance errors of the order of 10cm (=100mm) because the λ equals 10cm. Note that the IMU is not used for head orientation estimation because the gyroscope accumulates error but even the erroneous estimate can resolve the ambiguity. The 10cm (λ) of distance error would account to more than 20° of head orientation error which can be resolved by a noisy gyroscope as well. The algorithm [13, 12] also uses the gravity and magnetic north vectors to prevent the gyroscope's orientation error from diverging.

CHAPTER 5: IMPLEMENTATION DETAILS

5.1 PHYSICAL SETUP

Our implementation consists of four Decawave Trek1000 UWB devices [21]. Two of these radios are the transmitters at the cheat-piece which send packets in a time-shared way. The other two are the receivers at the headset that are also connected to the transmitters through a wire. We use a center frequency of *2GHz* with a bandwidth of *1GHz*. Further, we use MiniCircuits ZFRSC-123-S+ and ZFRSC-4-842-S+ splitters for splitting the signal into multiple paths. Each transmitter was programmed to send 20 packets per second using time-division multiple access (TDMA). At the receiver, the channel impulse response was captured and printed to the serial port using a USB connector. The CIRs from the receivers were stored on a Lenovo laptop running Microsoft Windows and were fed to the aforementioned four-stage processing pipeline programmed in Mathworks MATLAB.

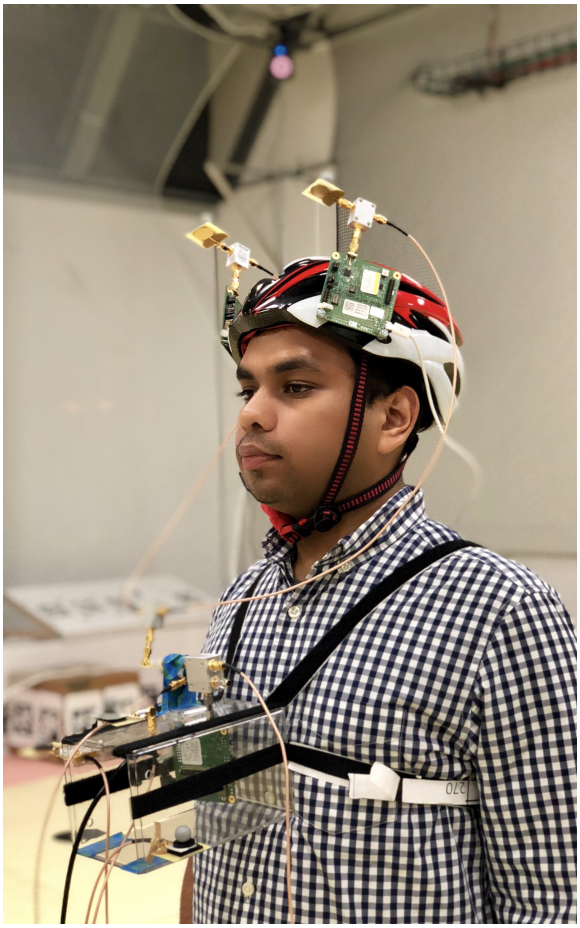

Figure 5.1: Experimental setup: human user wearing HeadTrack in ViCon room

Our prototype consists of a headset and a chest-piece that can be strapped on to the chest. The headset has two decawave UWB boards drilled onto a bicycle helmet and the chest-piece has two decawave UWB boards drilled to a plastic box with the antennas placed outside the box in LoS with the receivers. The receivers are connected to the transmitters using wires of varying lengths as the different lengths of the wires simulate different propagation delays between the transmitters and the receivers. The length of these wires is controlled by us while designing the system so that the propagation delay from each wire is previously known. Therefore, we can compensate for these pre-defined delays in our processing pipeline.

5.2 GROUND TRUTH COLLECTION

ViCon [24] is an IR camera-based tracking system and provides us with ground truth for HeadTrack. We place an IR reflecting marker on the top of each antenna in our system, along with three markers on the helmet, and one marker on the chest-piece.

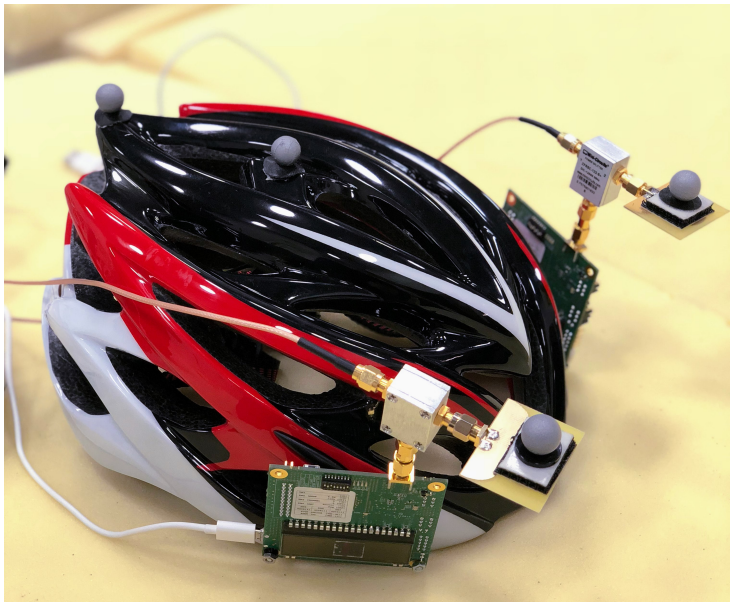

Figure 5.2: IR reflective ViCon markers on the HeadTrack headset

ViCon system uses multiple infra-red cameras at fixed positions in the room that can track the IR reflecting markers. ViCon provides localization data with an accuracy of 0.2mm [25] with an update rate of 240Hz, hence providing us a high-quality ground truth. Figure 5.2 shows the headset with the ViCon markers.

We perform numerous experiments in the ViCon lab at the CSL Studio including experiments on a mannequin head and a human user. For the mannequin head, we rotate the dummy at certain pre-defined angles and perform data collection along with estimation of distances. Figure 6.1 shows our ground truth collection and experimentation process using the mannequin head.

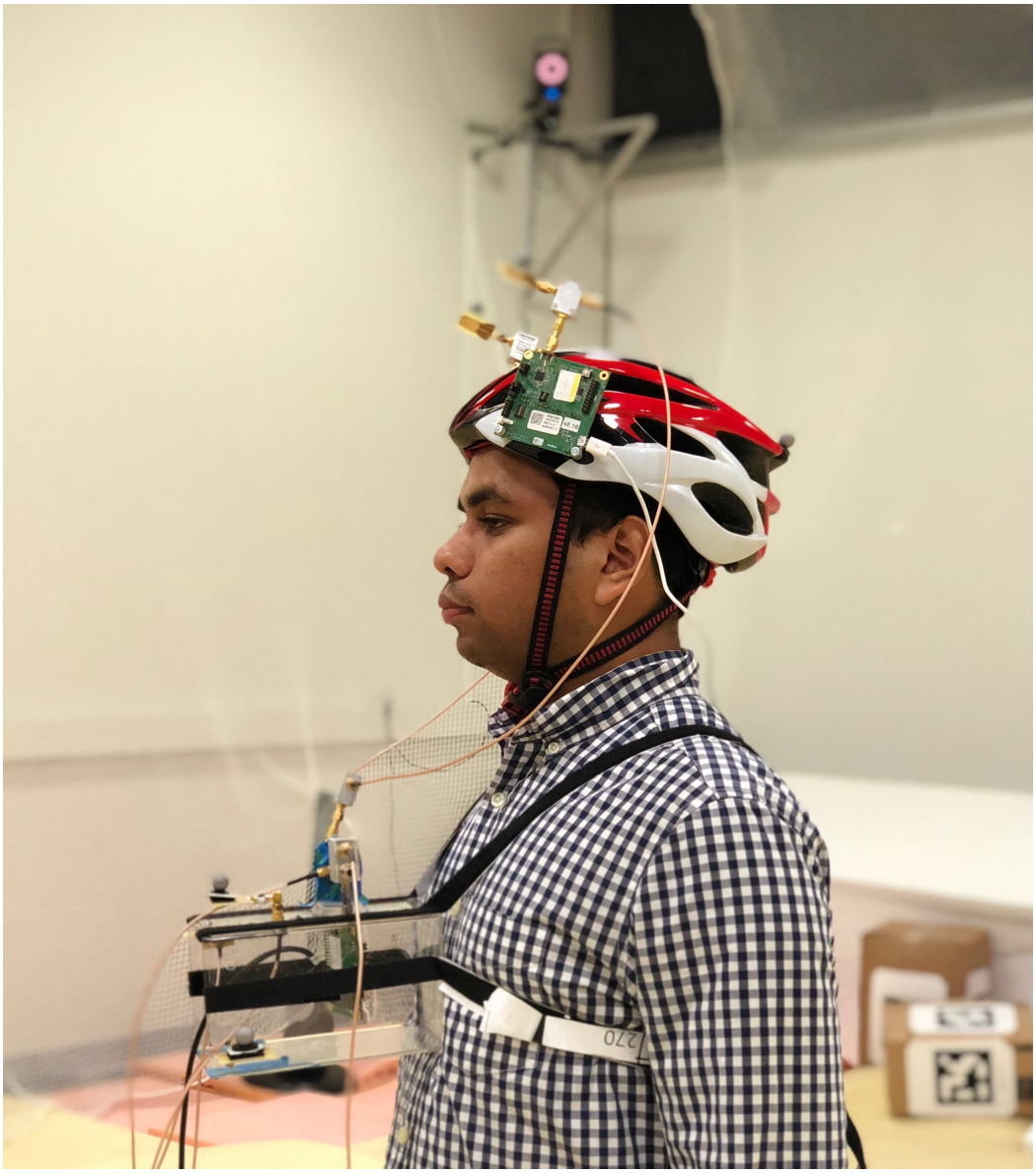

Figure 5.3: Human user wearing HeadTrack

We later perform experiments with human user and collect data for various head orientations. Figure 5.1 and Figure 5.3 shows our experimentation and data collection process with a human user.

CHAPTER 6: EVALUATION AND RESULTS

Evaluation of our system is primarily defined by the accuracy of the estimated Tx-Rx distance measurements. With our two pairs of distances between the transmitters and receivers, we can uniquely find the orientation of the head.

6.1 DISTANCE ESTIMATES WITH TIME OF FLIGHT

We start with using just the time-of-flight (ToF) measurements to estimate distances to evaluate the precision and stability of the ToF measurements. We observe that the peak detection algorithm along with the interpolation improves the precision to about 2cm.

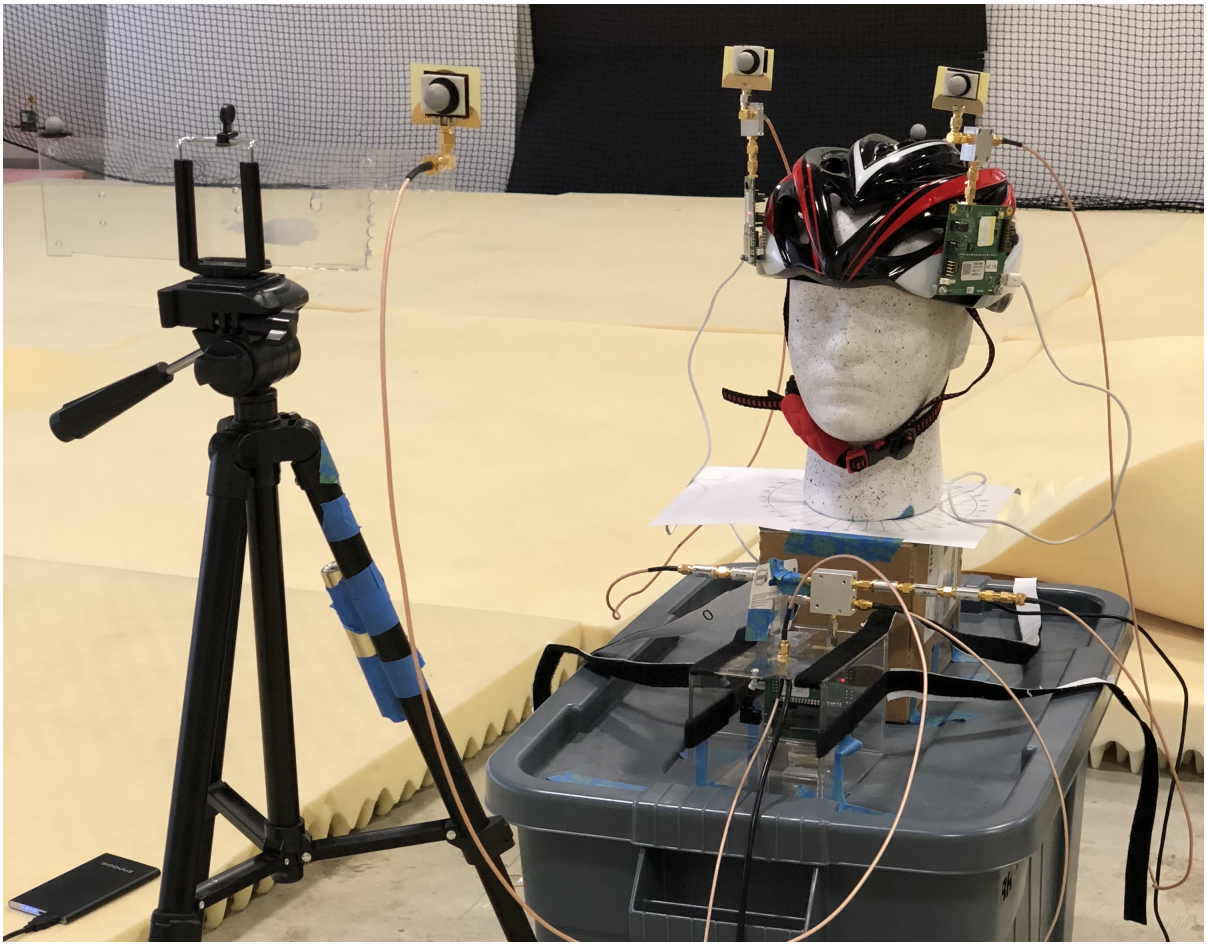

Figure 6.1: Mannequin experiment with HeadTrack

6.1.1 Experiment with Mannequin

Figure 6.1 shows the setup for the mannequin head experiments in the ViCon room. We rotate the head by a fixed degree and maintain a static position for around 30 seconds. Figure 6.2 shows the results for estimated distances (in mm) without phase refinement. The four colors on the plot represent the four Tx-Rx distances, the transition period in-between changing orientation of the head has been removed from this plot. From the plot, we observe that for each orientation ToF measurements fluctuate around 2cm.

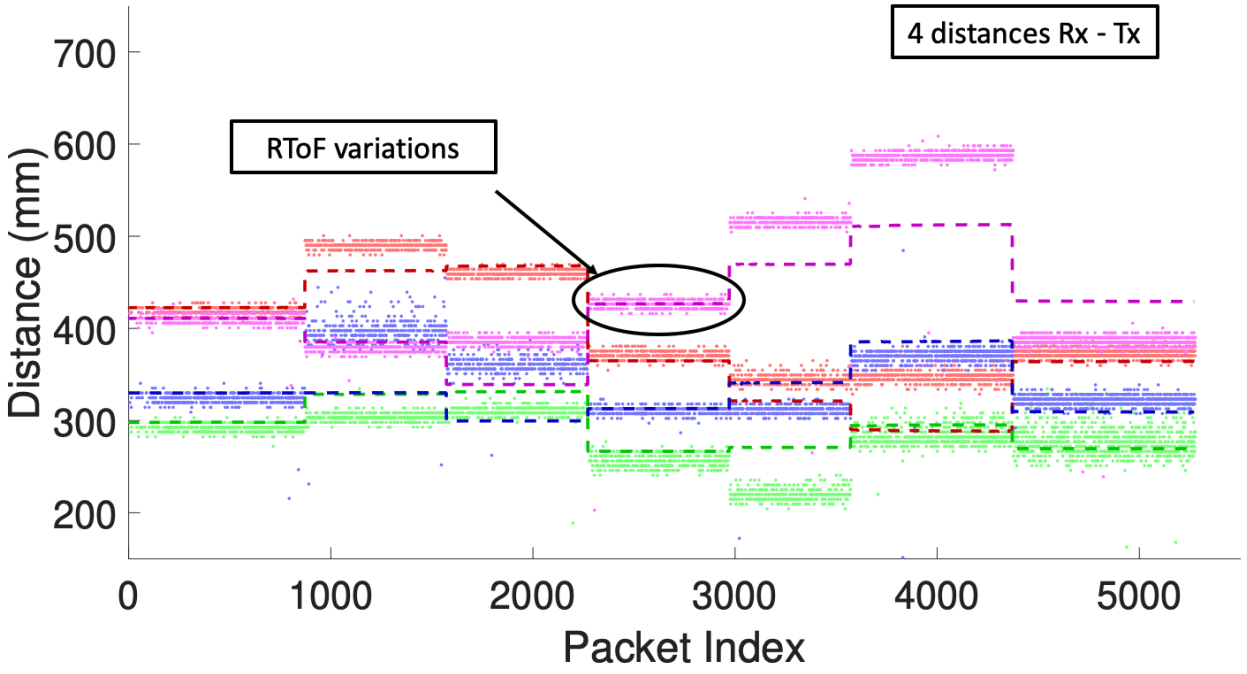

Figure 6.2: Mannequin experiment: Distance estimates using time-of-flight measurements (scatter points) without using phase refinement compared with the Ground Truth (dotted lines)

6.1.2 Experiment with Humans

During the human experiments, we constant move our head in different orientations. However, to be able to draw a parallel with the mannequin experiment, we also move the head at certain degrees and maintain static positions. Figure 6.3 distance estimates for the two receivers from a single transmitter. We plot only one of the two pairs of distances for clarity. Since human body is almost 60% water, we observe that human body causes significantly more multipath. Due to the reflections from the body itself, we observe that

Figure 6.4 shows stronger ToF variations in case of human experiments.

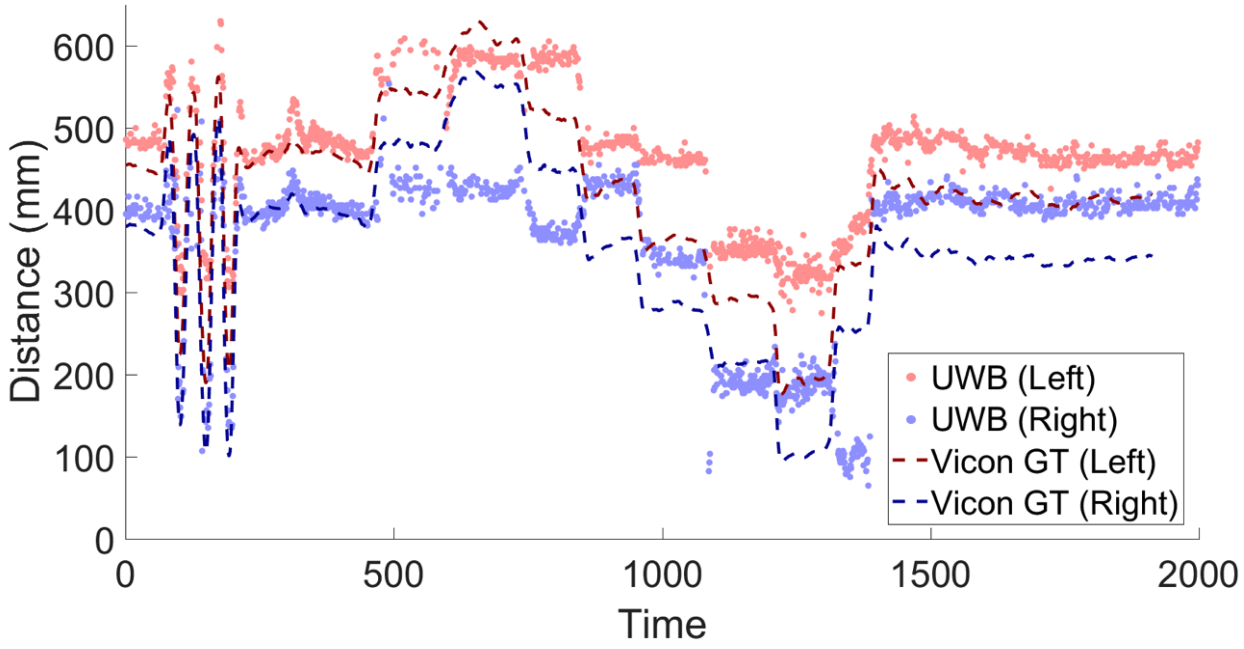

Figure 6.3: Human experiment: Distance estimates using ToF measurements without using phase refinement compared with the Ground Truth

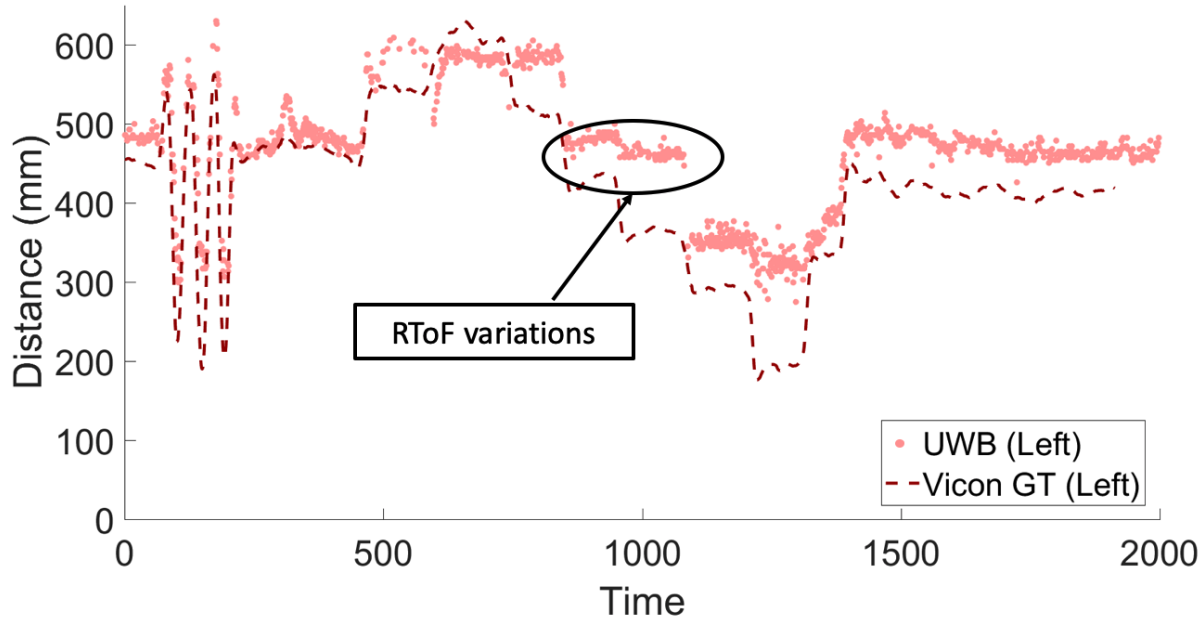

Figure 6.4: Human experiment: ToF shows stronger variations due to body multipath

6.2 REFINEMENT WITH PHASE

While we have improved ToF precision, we direct our focus to using the carrier phase to further refine the ToF measurements. Recall that the relative phase between our two peaks in the CIR is a function of the distance between the two impulses that generated those peaks. We use this phase information to *snap* the ToF measurement to the *closest value* that satisfies $n\lambda + \phi$, where ϕ is the measured phase at the receiver.

6.2.1 Experiment with Mannequin

Figure 6.5 shows the refined ToF measurements using phase information. *Snapping* the measurement to the closest possible value of $n\lambda + \phi$ that satisfies the measure phase reduces the variations in ToF.

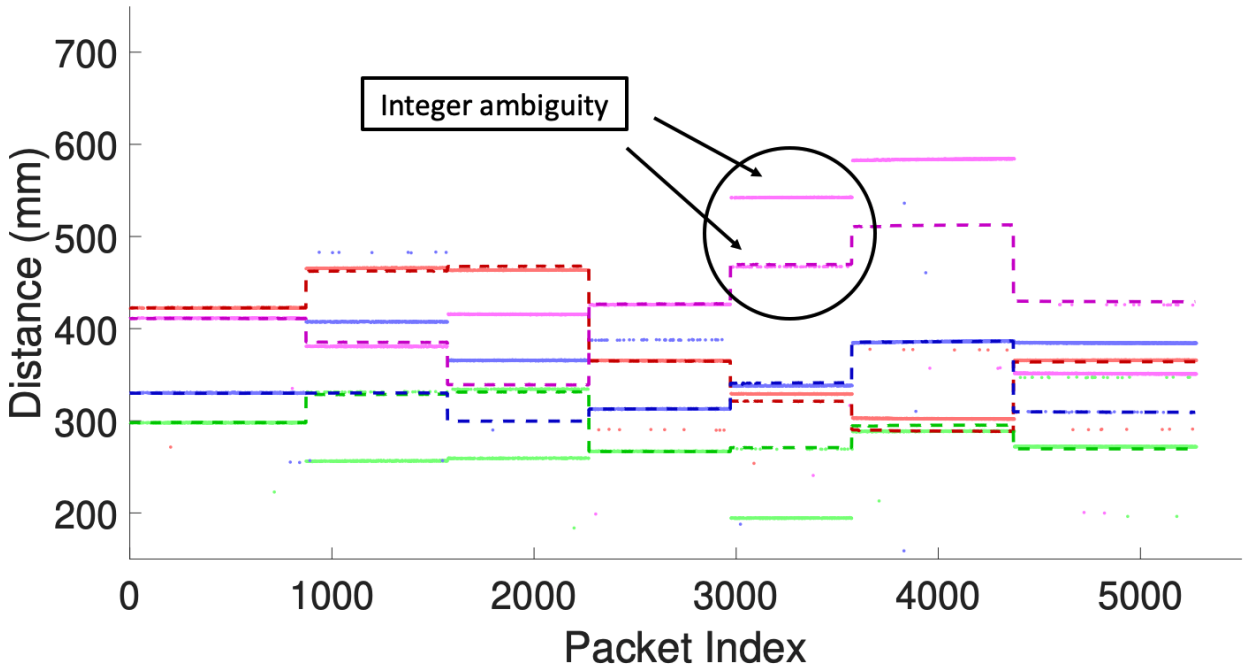

Figure 6.5: Mannequin experiment: Distance estimated using ToF with phase refinement (scatter points) compared with the Ground Truth (dotted lines)

The error is drastically reduced, however, as observed in the distance plot there exists an **integer ambiguity** that can snap the ToF measurement off by a distance of λ.

6.2.2 Experiment with Humans

Figure 6.6 shows the refined ToF measurements using the phase information in case of humans. Due to larger multipath and resulting variation in ToF, the integer ambiguity is worse in this case. This motivates us to look for new solutions to solve the ambiguities.

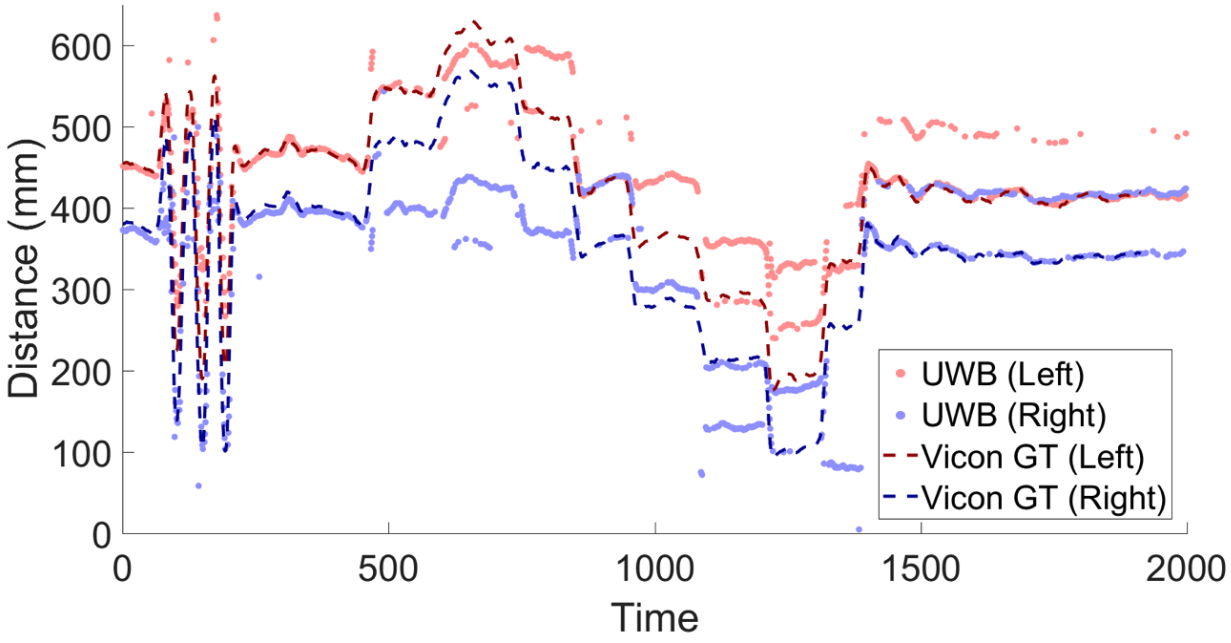

Figure 6.6: Human experiment: Distance estimated using ToF with phase refinement compared with the Ground Truth

6.3 SOLVING INTEGER AMBIGUITY WITH IMU

Recall from stage 4 of our system design, we use the IMU to find the orientation of the helmet and solve the integer ambiguity. The IMU orientation helps us find the Euler angles that further resolves the ambiguity. Figures 6.5 and 6.7 show the integer ambiguity in our system. We plot the distance estimates after resolving the ambiguity in Figure 6.8.

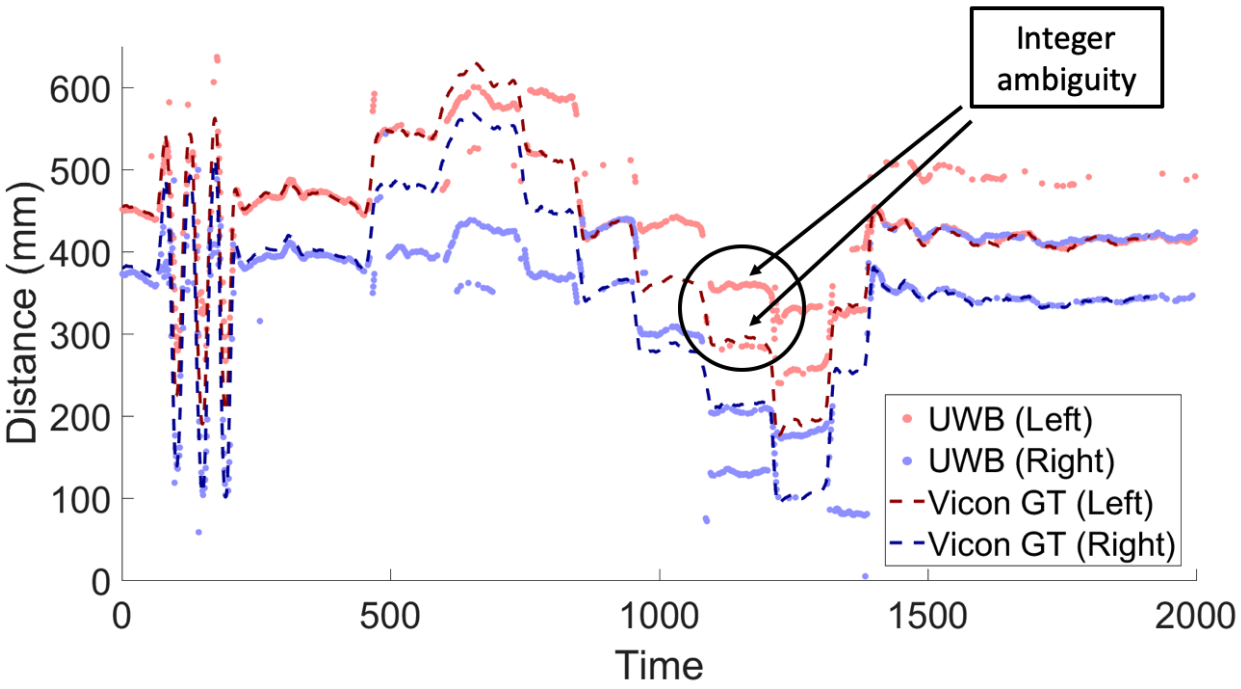

Figure 6.7: Human experiment: Distance estimates show integer ambiguity (phase refinement is off by λ)

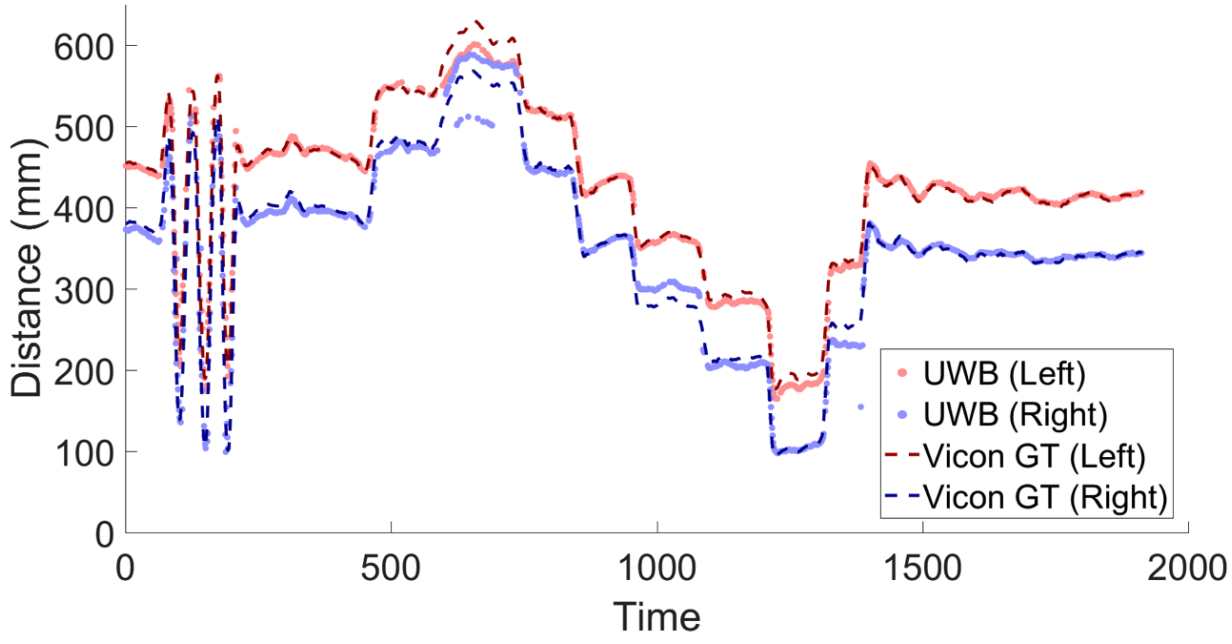

Figure 6.8: Human experiment: Integer ambiguity is resolved using the Euler angles from the IMU orientation estimate

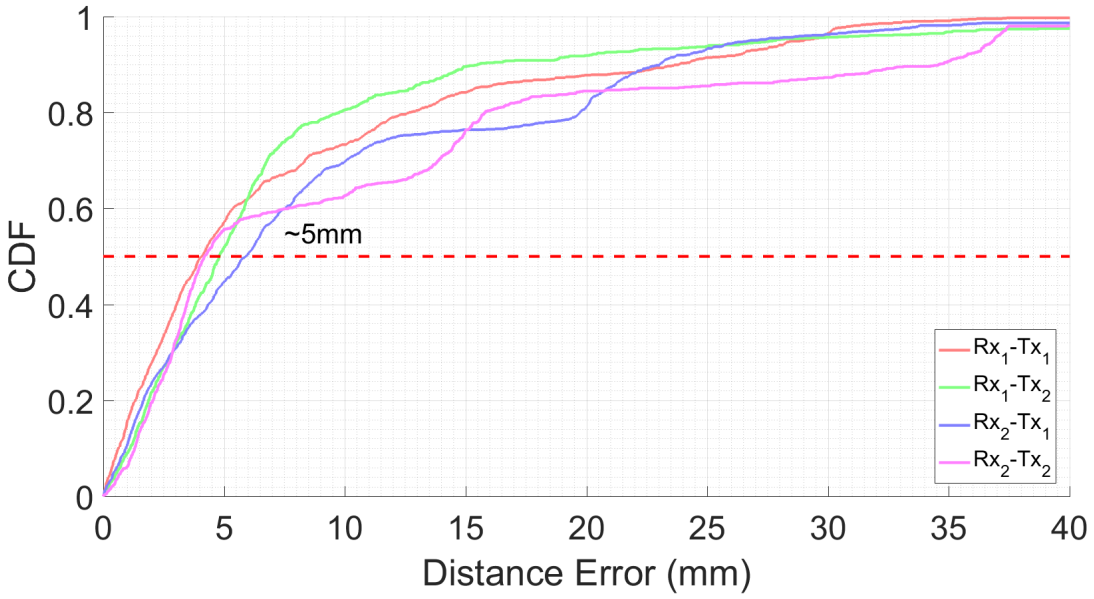

Figure 6.9: HeadTrack has a median error of 5mm for the distance estimates. All four Tx-Rx distance estimates show similar estimation errors around the 50th percentile.

After the integer ambiguity is resolved, we calculate the absolute error over the temporal data to plot a cumulative density function (CDF). From Figure 6.9 we observe that at the 50th percentile distance estimate error is around 5mm. Recall from our earlier discussion that UWB ranging typically gives us errors of the order of 10cm. With the reference wired path and the phase refinement, we are able to reduce the median distance estimate error to less than a centimeter.

What is the source of ToF error? It is imperative to understand the source of ToF error. The core source of inaccuracy stems from the presence of the multipath in the system. For example, the observed channel impulse response for one of the Tx-Rx packets where estimated ToF is significantly wrong is shown in Figure 6.10. Note that the two close peaks at the wireless path (shown in the blue box) represent multipath and affects the results of the peak detection algorithm. In general, we see that the phase is typically stable under the peaks but that may also be not the case in scenarios involving strong multipath.

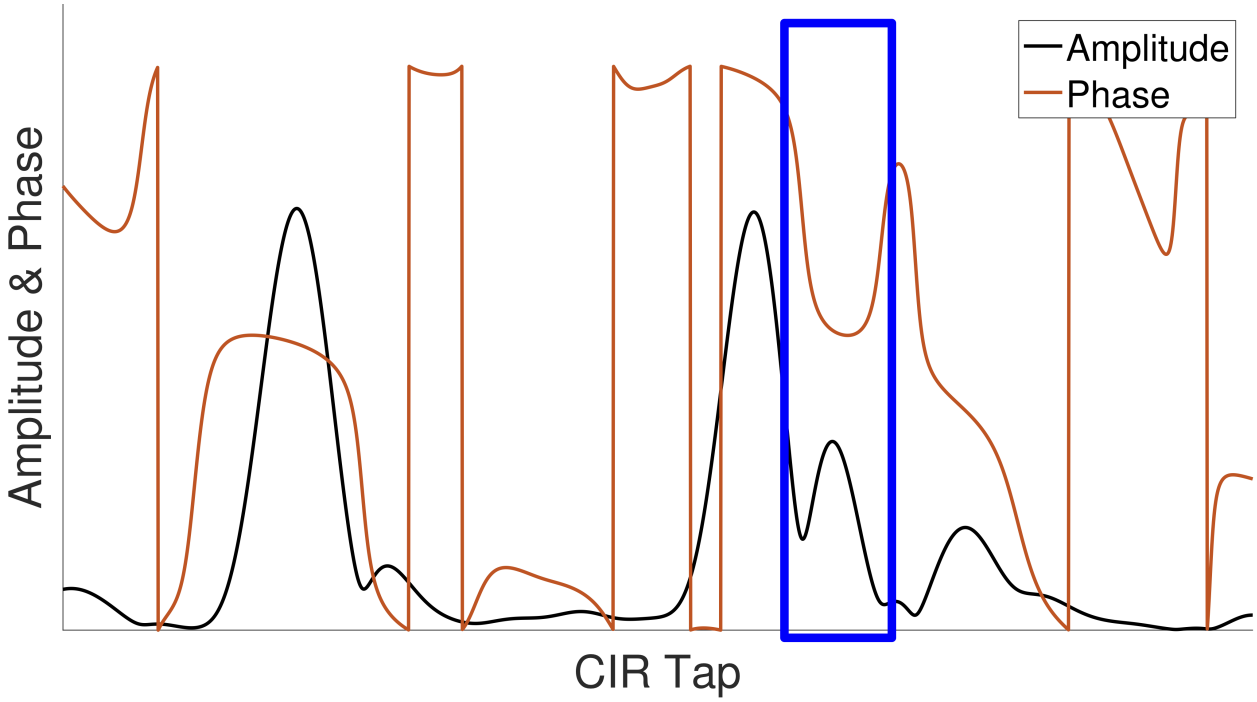

Figure 6.10: Strong multipath can pollute the peak at the wireless channel (blue box)

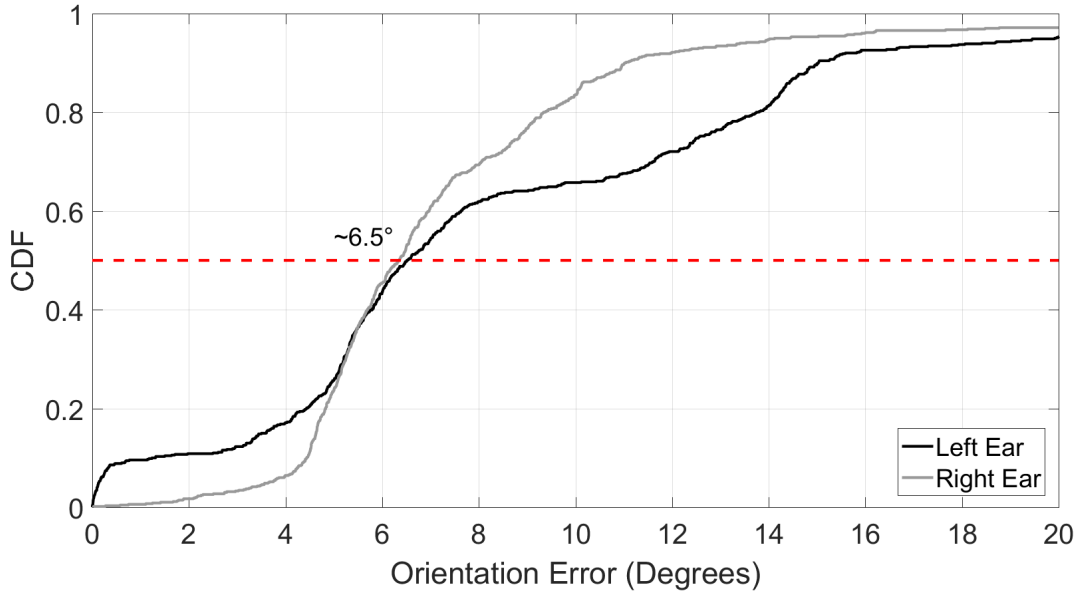

Figure 6.11: HeadTrack has a median error of 6.5° in orientation estimate

Our ultimate objective is to be able to translate these four distances into unique head orientation value that is defined by $\langle yaw, pitch, roll \rangle$ with respect to the origin as defined in

Figure 4.6.

We project our distance estimates into the 3D space and use the MATLAB solver to uniquely find the head orientation at every point. We also project the ground truth distances from the ViCon into the 3D space and use the same deterministic solver to find the ground truth for head orientation. We then compare the two values and plot the CDF for the orientation estimate error and observe that at 50th percentile the error is around 6.5° as shown in Figure 6.11.

CHAPTER 7: CONCLUSION

7.1 CONTRIBUTION

In this work, we explore the possibility to use RF signals to track the orientation of the user's head. While UWB radios have always been used to perform large area localization where errors of the order of 10cm can suffice, we focus on fine grained localization with sub-cm error in this work. We show that it is feasible to develop a wearable that can work with headsets (like headphones) to precisely track the head orientation with a median error of about 6.5°. Our solution not only solves the problem with an error that would suffice for most head tracking applications but also enables portability and mobility for the user.

7.2 DISCUSSION

What would be the cost of HeadTrack? The total cost we incurred in creating the prototype was under $1000. The reprogrammable Decawave platform that we use to send UWB signals accounts for a major portion of the cost, which can be significantly reduced in production design. Further, the cost of components can be made negligible by splitting and delaying signals in PCD itself. We expect these production-level developments to bring down the cost of this system under $100. It's also important to note that we do not use an expensive IMU in our prototype.

Can the HeadTrack be implemented using two UWB devices? It is possible to replace the two receivers with just one device with two antennas. Similarly, two transmitters can be replaced by a single device with two antennas. However, practically, when a single transmitter and receiver is used - it is important to keep the two CIRs untangled. In our case, we introduced artificial delays to the signal by using long wires, therefore, that would be logically challenging. However, in production, delays can be introduced using delay components making HeadTrack possible with just two UWB devices.

Can the calibration step be eliminated? HeadTrack measures the relative time of flight to estimate the changes in the distances. This will vary for each person and will also depend on where the chest-piece is worn every time. However, as the system is being used, it's possible to learn these parameters over time. The initial calibration process will just scale the extreme values of this learned model.

Can HeadTrack track positional motion of the user? In this work, we do not target the mobility of the users and the position tracking of the their body. However, we believe a lot of work has been done in localization and tracking users' positional mobility [10, 19, 13, 12, 4]. Adding static antennas as anchors near the position of the user should be able to solve the problem. However, we have developed a system that can independently estimate head orientation without getting affected by the positional motion of the user.

7.3 FUTURE WORK

We envision this solution to be more robust to multipath and the ambiguities. Fusing filtering and tracking algorithms like the Hidden Markov Models (HMM) or the Kalman Filter with HeadTrack can surely make the system sturdier against the ambiguities. The latest Decawave boards are also able to estimate the angle of arrival (AoA) of the signal. It may be possible to learn and model the multipath from the human body and environment using the RSSI and AoA given its temporal nature. Once modeled, it may be possible to shield against multipath by subtracting it in real time. However, we do not explore this problem in this work.

In this work, we have not focussed on developing a production quality prototype. Naturally a lot more work is required to make it a production device. In the prototype, we use the large Decawave development UWB boards, however, in production development the radios can be as small as 2mm x 2mm. We have also not focussed on conserving battery - the ranging packet rate can be dynamically modified according to the readings from the IMU. When the IMU reads a vigorous change in the head position, the packet rate can automatically increase to precisely track the motion. We use long wires to simulate delays which can be done using delay lines in production. We can also employ other ranging radios like mmWave which can provide higher bandwidth and resolution. We expect the size and cost of the device in production to be much smaller and cheaper than our prototype.

7.4 CONCLUSION

Tracking head orientation is a hard problem [14] and the current solutions make it an expensive one as well. While most current solutions use very expensive hardware (lasers, cameras, and expensive IMUs), we explore the possibility to develop a system that not only

enables portability but can also be significantly cheaper than the current solutions. We demonstrate that it is feasible to make a wearable that can use RF signals to estimate the head orientation of the user *independently* of the user's body motion. HeadTrack is able to decouple the head motion and body motion because it uses the transmitter on the torso as an "anchor".

Our results show a median error of 6.5° which may not be good enough for a few applications that require very high accuracy (like AR/VR systems) but will suffice for most head orientation tracking applications. We believe, HeadTrack provides a wearable, occlusion-free, portable, and cost-effective solution to the problem of head orientation tracking with a bounded and non-diverging error.

REFERENCES

[1] TSA, "How mmwave and backscatter scanners work?" https://www.tsa.gov/blog/2008/05/27/which-it-millimeter-wave-or-backscatter/.

[2] J. A. Gutierrez, E. H. Callaway, and R. Barrett, *IEEE 802.15.4 Low-Rate Wireless Personal Area Networks: Enabling Wireless Sensor Networks.* New York, NY, USA: IEEE Standards Office, 2003.

[3] P. Bahl, V. N. Padmanabhan et al., "Radar: An in-building rf-based user location and tracking system."

[4] D. Vasisht, A. Jain, C.-Y. Hsu, Z. Kabelac, and D. Katabi, "Duet: Estimating user position and identity in smart homes using intermittent and incomplete rf-data," *Proc. ACM Interact. Mob. Wearable Ubiquitous Technol.*, vol. 2, no. 2, pp. 84:1–84:21, July 2018. [Online]. Available: http://doi.acm.org/10.1145/3214287

[5] A. Dhekne, M. Gowda, Y. Zhao, H. Hassanieh, and R. Roy Choudhury, "LiquID: A Wireless Liquid IDentifier," *To appear in MobiSys*, 2018.

[6] J. F. James, R. S. Sternberg, and S. A. Rice, "The design of optical spectrometers," *Physics Today*, vol. 23, p. 55, 1970.

[7] H. Wang, C. Mao, H. He, M. Zhao, T. S. Jaakkola, and D. Katabi, "Bidirectional inference networks: A class of deep bayesian networks for health profiling," *arXiv preprint arXiv:1902.02037*, 2019.

[8] F. Adib, Z. Kabelac, D. Katabi, and R. C. Miller, "3d tracking via body radio reflections," in *11th {USENIX} Symposium on Networked Systems Design and Implementation ({NSDI} 14)*, 2014, pp. 317–329.

[9] A. Alanis, , , R. Gilad-Bachrach, and D. Lymberopoulos, "3d gesture recognition through rf sensing," June 2014. [Online]. Available: https://www.microsoft.com/en-us/research/publication/3d-gesture-recognition-through-rf-sensing/

[10] A. Dhekne, U. J. Ravaioli, and R. R. Choudhury, "P2ploc: Peer-to-peer localization of fast-moving entities," *Computer*, vol. 51, no. 10, pp. 94–98, October 2018.

[11] M. Gowda, A. Dhekne, S. Shen, R. R. Choudhury, L. Yang, S. Golwalkar, and A. Essanian, "Bringing iot to sports analytics," in *14th {USENIX} Symposium on Networked Systems Design and Implementation ({NSDI} 17)*, 2017, pp. 499–513.

[12] P. Zhou, M. Li, and G. Shen, "Use it free: Instantly knowing your phone attitude," in *Proceedings of the 20th Annual International Conference on Mobile Computing and Networking*, ser. MobiCom '14. New York, NY, USA: ACM, 2014. [Online]. Available: http://doi.acm.org/10.1145/2639108.2639110 pp. 605–616.

[13] S. Shen, M. Gowda, and R. Roy Choudhury, "Closing the gaps in inertial motion tracking," in *Proceedings of the 24th Annual International Conference on Mobile Computing and Networking*, ser. MobiCom '18. New York, NY, USA: ACM, 2018. [Online]. Available: http://doi.acm.org/10.1145/3241539.3241582 pp. 429–444.

[14] G. Welch and E. Foxlin, "Motion tracking: no silver bullet, but a respectable arsenal," *IEEE Computer Graphics and Applications*, vol. 22, no. 6, pp. 24–38, Nov 2002.

[15] D. F. DeMenthon and L. S. Davis, "Model-based object pose in 25 lines of code," in *European conference on computer vision*. Springer, 1992, pp. 335–343.

[16] D. C. Niehorster, L. Li, and M. Lappe, "The accuracy and precision of position and orientation tracking in the htc vive virtual reality system for scientific research," *i-Perception*, vol. 8, no. 3, p. 2041669517708205, 2017. [Online]. Available: https://doi.org/10.1177/2041669517708205

[17] S. M. LaValle, A. Yershova, M. Katsev, and M. Antonov, "Head tracking for the oculus rift," in *2014 IEEE International Conference on Robotics and Automation (ICRA)*, May 2014, pp. 187–194.

[18] E. Foxlin, "Inertial head-tracker sensor fusion by a complementary separate-bias kalman filter," in *Proceedings of the IEEE 1996 Virtual Reality Annual International Symposium*, Mar 1996, pp. 185–194, 267.

[19] J. A. Corrales, F. A. Candelas, and F. Torres, "Hybrid tracking of human operators using imu/uwb data fusion by a kalman filter," in *2008 3rd ACM/IEEE International Conference on Human-Robot Interaction (HRI)*, March 2008, pp. 193–200.

[20] B. Campbell, P. Dutta, B. Kempke, Y.-S. Kuo, and P. Pannuto, "Decawave: Exploring state of the art commercial localization," *Ann Arbor*, vol. 1001, p. 48109, 2015.

[21] DecaWave, "Decawave," http://www.decawave.com/.

[22] A. Alarifi, A. Al-Salman, M. Alsaleh, A. Alnafessah, S. Al-Hadhrami, M. A. Al-Ammar, and H. S. Al-Khalifa, "Ultra wideband indoor positioning technologies: Analysis and recent advances," *Sensors*, vol. 16, no. 5, p. 707, 2016.

[23] DecaWave, "DW1000 User Manual," https://decawave.com/content/dw1000-user-manual.

[24] Vicon, "Vicon," https://www.vicon.com/.

[25] P. Merriaux, Y. Dupuis, R. Boutteau, P. Vasseur, and X. Savatier, "A study of vicon system positioning performance," *Sensors*, vol. 17, no. 7, p. 1591, 2017.